Journal of Structural Geology, Vol. 11, No. 7, pp. 827 to 846, 1989
Printed in Great Britain

0191-8141/89 $03.00 + 0.00

The frictional properties of a simulated gouge having a fractal particle distribution

RONALD L. BIEGEL*, CHARLES G. SAMMIS

Department of Geological Sciences, University of Southern California, Los Angeles, CA 90087-0740, U.S.A.

and

JAMES H. DIETERICH

Center for Earthquake Studies, United States Geological Survey, Menlo Park, CA 904025, U.S.A.

(*Received* 4 *November* 1988; *accepted in revised form* 27 *April* 1989)

Abstract—The frictional properties of a layer of simulated Westerly granite fault gouge sandwiched between sliding blocks of Westerly granite have been measured in a high-speed servo-controlled double-direct shear apparatus. Most gouge layers were prepared to have a self-similar particle distribution with a fractal dimension of 2.6. The upper fractal limit was varied between 45 and 710 μm. Some gouges were prepared with all particles in the range between 360 and 710 μm. In each experiment the sliding velocity was cyclically alternated between 1 and 10 μm s^{-1} and the coefficient of friction μ and its transient parameters a, b and D_c were measured as functions of displacement. In addition to the particle size distribution, the following experimental variables were also investigated: the layer thickness (1 and 3 mm), the roughness of the sliding surfaces (Nos 60 and 600 grit) and the normal stress (10 and 25 MPa). Some of the sample assemblies were epoxy impregnated following a run so the gouge structure could be microscopically examined in thin section. We observed that gouges which were initially non-fractal evolved to a fractal distribution with dimension 2.6. Gouges which had an initial fractal distribution remained fractal. When the sliding blocks had smooth surfaces, the coefficient of friction was relatively low and was independent of the particle distribution. In these cases, strong velocity weakening was observed throughout the experiment and the transient parameters a, b and D_c remained almost constant. When the sliding blocks had rough surfaces, the coefficient of friction was larger and more dependent on the particle distribution. Velocity strengthening was observed initially but evolved to velocity weakening with increased sliding displacement. All three transient parameters changed with increasing displacement. The a and b values were about three times as large for rough surfaces as for smooth. The characteristic displacement D_c was not sensitive to surface roughness but was the only transient parameter which was sensitive to the normal stress. For the case of rough surfaces, the coefficient of friction of the 1 mm thick gouge was significantly larger than that for the 3 mm thick layers. Many of these observations can be explained by a micromechanical model in which the stress in the gouge layer is heterogeneous. The applied normal and shear stresses are supported by 'grain bridges' which span the layer and which are continually forming and failing. In this model, the frictional properties of the gouge are largely determined by the dominant failure mode of the bridging structures.

INTRODUCTION

THE wall rocks in most natural fault zones are separated by a layer of cataclastic rock. At shallow depths the cataclastic material often consists of a non-cohesive rock flour called gouge. In some cases gouge is mineralogically altered by ground water to clay, but in others this alteration is negligible (Wu *et al.* 1975, Anderson *et al.* 1982). Sammis *et al.* (1987) and Sammis & Biegel (in press) measured the particle size distribution of unaltered gouge from the Lopez fault, a thrust fault associated with the San Gabriel fault zone in southern California. They observed that over a range of particle diameters from 10 μm to 1 cm the gouge was self-similar with a fractal dimension of $D = 2.6 \pm 0.1$. Since this fractal dimension characterizes a distribution which minimizes the number of nearest neighbors of the same size *at all scales*, they proposed a comminution mechanism in which each particle's fracture probability is determined solely by the relative size of its nearest neighbors, and specifically does not depend on the particle's size or its mineralogy. Like other processes which generate fractal patterns, comminution in dense aggregates (where the particles are loaded by neighboring particles) is controlled by the interaction between different scales, and normal considerations of particle strength become unimportant. Other examples of this type of 'constrained comminution' such as fragmentation by underground explosions have been documented by Turcotte (1986).

The experiments described in this study had two objectives. The first was to test the proposed comminution mechanism by observing the evolution of an initially uniform particle size distribution with increasing shear strain. The second was to understand the significance of the fractal particle distributions observed in natural fault zones for their frictional constitutive behavior. The friction experiments described below extended the earlier work of Dieterich (1981) on the effect of surface roughness and gouge particle size on the constitutive behavior. Measurements were made using the same high-speed servo-controlled double-direct shear apparatus described in that paper. The sliding blocks were of Westerly granite with layers of simulated gouge pre-

*Present address: Lamont-Doherty Geological Observatory of Columbia University, Palisades, NY 10964, U.S.A.

pared from crushed and sieved Westerly granite. The principal difference is that the present experiments focused on simulated gouges that were prepared to be self-similar with a fractal dimension of 2.6 and that had different upper fractal limits of grain sizes. The experiments were initially designed to test the hypothesis that the characteristic distance parameter in rate- and state-dependent friction laws is controlled by the upper fractal limit of the fractal gouge (Sammis & Biegel in press). The other transient constitutive parameters were also measured as a function of sliding displacement, and additional experimental variables such as layer thickness and normal stress were also varied. Optical photomicrographs of the deformed gouge layers were prepared in order to correlate differences in constitutive behavior with observed differences in the gouge microstructure.

Most of our experiments employed several step changes in loading velocity to evaluate both transient and steady-state dependences of fault strength on slip speed. A portion of the data from a typical experiment is shown in Fig. 1. The slip speed was generally alternated between 1 and 10 μm s^{-1}. Experiments were also conducted at constant slip speed to evaluate the dependence of overall strength on sliding displacement. The velocity-stepping experiments generally produced a response that is ideally represented in the lower portion of Fig. 1. A step increase of sliding speed results in a sudden increase in sliding resistance which is followed by a displacement-dependent decrease of strength to a new steady state value. A step decrease in loading rate produces a symmetric response. Following a step down in slip speed, the sliding resistance quickly drops and then undergoes a displacement-dependent increase to a new steady state value. If the steady state friction increases with increasing velocity, then the behavior is commonly referred to as velocity strengthening and conversely if the strength decreases it is called velocity weakening. Both velocity strengthening and velocity weakening are observed in these experiments.

In practice, these transient and residual velocity effects are generally superimposed on long-term displacement-dependent changes of sliding resistance. Hence, all measurements of the effects of slip speed on constitutive parameters reported here were made relative to long-term trends. Except for initial measurements at small cumulative displacements, results for velocity stepping are made under conditions in which the coefficient of friction at constant velocity varies by 0.002 mm^{-1} or less.

The results of our experiments are interpreted in the context of a state-variable constitutive law as proposed by Dieterich (1979a,b, 1981) and modified by Ruina (1983). Several different, but essentially equivalent, formulations are in use and Okubo & Dieterich (1986) discuss the relationships among the different formulations. For our discussion we employ the simplified form:

$$\mu = \mu_0 + b \log_{10} \frac{\theta}{\theta_0} + a \log_{10} \frac{V}{V_0}, \qquad (1)$$

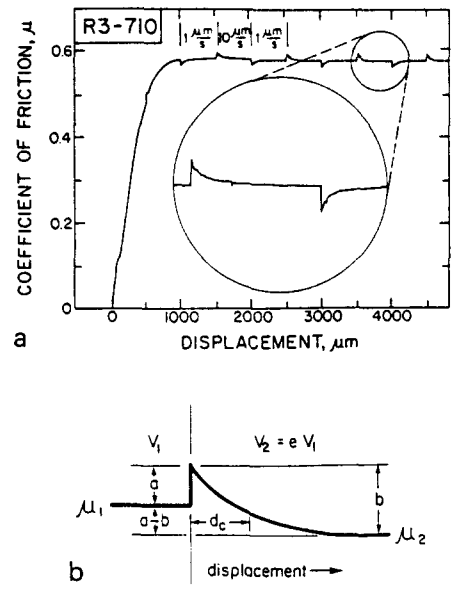

Fig. 1. (a) Part of the data from a typical velocity-stepping experiment. The coefficient of friction is plotted as a function of the total sliding displacement. The sliding velocity was cycled between 1 and 10 μm s^{-1} as indicated. The transient response to a velocity increase and decrease is shown in the enlarged inset. (b) The idealized friction response to a step increase in sliding velocity. Parameter a measures the instantaneous change in friction while b measures the relaxation which occurs over the characteristic distance D_c defined in the text. The difference $a - b$ gives the difference in steady-state friction. If $a - b > 0$, then the system is said to velocity strengthen. If $a - b < 0$ (as shown here) the system is said to velocity weaken.

where μ is the coefficient of friction, V is the slip speed, θ is the state variable and μ_0, a, b, θ_0 and V_0 are constants. The normalizing constants θ_0 and V_0 are arbitrary and may be combined with μ_0 to yield:

$$\mu = \mu_0 + a \log_{10} \theta + b \log_{10} V. \qquad (2)$$

The state variable θ depends upon sliding speed and sliding history. Different but related laws have been proposed to represent the history-dependence of θ (Rice & Gu 1983, Tullis & Weeks 1986). All share the characteristics that there is some steady-state value of θ that depends on slip speed:

$$\theta_s = \frac{D_c}{V}, \qquad (3)$$

and that under conditions where $\theta \neq \theta_s$, θ will evolve toward the instantaneous value of θ_s over the characteristic slip distance D_c. It has been found that D_c depends on roughness and the presence of simulated gouge separating the surfaces.

In the idealized response shown in the lower portion of Fig. 1 note that a and b are given directly by the amplitude of the jump in the coefficient of friction at the time of a velocity step and by the amplitude of the displacement-dependent decay to the residual friction, respectively. The decay distance is proportional to D_c. In practice, however, the finite apparatus stiffness precludes an instantaneous jump of slip speed and absolute control at a constant speed if the stress is varying. Consequently, for a step in loading velocity, some evolution of θ occurs before the new sliding speed is reached.

This in turn decreases the amplitude of the observed height of the initial jump in strength relative to the ideal case and also tends to increase the sliding distance to reach a new steady state. In cases where the stiffness problem is severe, reduction of the experimental data to obtain independent estimates of a, b and D_c requires simulations which take into account the machine stiffness effects. In our apparatus the loading stiffness is quite high compared to the velocity-controlled stress changes and characteristic displacement and we report the data for a, b and D_c measured directly from the experimental curves.

In the set of experiments described below, μ and its transient parameters a, b and D_c were measured as a function of displacement. Four additional experimental variables were changed in order to evaluate their effect on these constitutive parameters. These variables are: (1) the normal stress (10 and 25 MPa); (2) the surface roughness of the sliding blocks (rough = No. 60 and smooth = No. 600 grit); (3) the upper fractal limit of the gouge (45, 90, 180, 360 and 710 μm); and (4) the layer thickness (1 and 3 mm). While many of our results confirm those found by Dieterich (1981), some are new. New observations include a systematic dependence of μ on the upper fractal limit of the gouge, and on the layer thickness for the case of rough surfaces. The transient parameters a and b were found to be sensitive to the surface roughness while D_c was most sensitive to the normal stress.

Many of the experimental observations described below cannot be explained in the context of continuum mechanics. Rather, they suggest that a model in which stress is transmitted through the gouge by a continually changing network of 'grain bridges' may offer a better description of the micromechanics of gouge deformation.

EXPERIMENTAL PROCEDURE

A single piece of Westerly granite was used to prepare all of the sliding blocks and fault gouge used in these experiments. Sets of three blocks were cut and polished to make the sandwich configuration for the double-shear apparatus described in Dieterich (1978) and shown schematically in Fig. 2. Each block was given a 'rough' or 'smooth' surface by hand lapping with No. 60 or No. 600 silicon carbide, respectively. Before each run the blocks were inspected to ensure that no cracks or other imperfections had appeared which could affect the data.

The remainder of the uncut Westerly granite was crushed and sieved to make gouge. Each size fraction was made separately to ensure that each had the same composition. The fractions were classified by their particle size diameters which differed by factors of two ranging from smallest (less than 45 μm) to largest (360–710 μm). The different size fractions were then mixed to make artificial gouges with self-similar particle size distributions having a fractal dimension of 2.6. This dimension was produced by adding $\frac{1}{6}$ the number of particles

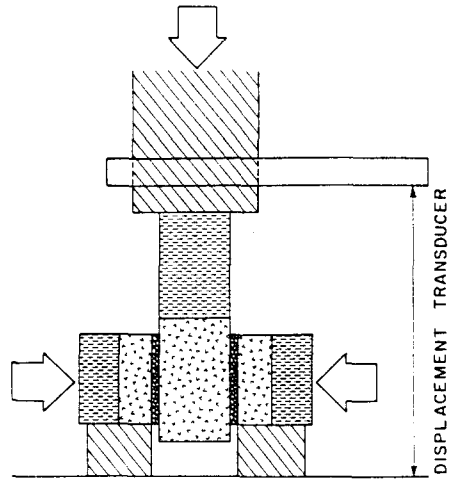

Fig. 2. Sketch of the servo-controlled double-direct shear apparatus. Outer sample block dimensions are 5.0 × 5.0 × 1.9 cm.

(estimated by weight) for each factor of 2 increase in particle size. Each batch thus consisted of a base gouge having grains less than 45 μm diameter to which was added the proper proportion of each larger size fraction up to the desired particle size cutoff. The finished batch was classified by the diameter of its largest size fraction in microns (see Table 1). The gouge was placed between the sliding blocks in layers 1 or 3 mm thick using a special form to make the thickness uniform and reproducible.

A typical experiment consisted of 10 mm of total simple-shear displacement divided into 20 segments of 500 μm each. The sliding velocity was alternated between 1 and 10 μm s^{-1}. A total of 47 experiments was run which may be broken down into four sets. First, the frictional properties were investigated in 27 runs constituting the R1, R3 and S3 series summarized in Table 1. Each run is identified by a code in which the first letter denotes the surface as rough (R) or smooth (S), the next number shows the gouge layer thickness as 1 or 3 mm, and the final number gives the diameter of the upper fractal limit in microns. Changes in the particle size distribution and geometry were investigated in a second set of 13 runs constituting the R_e3 and S_e3 series. The subscript 'e' indicates these samples were vacuum impregnated with epoxy and cut into thin sections for optical and SEM (scanning electron microscope) observation. The total displacement in this series was varied in order to observe the evolution of the particle structure within the gouge. A clamp was attached to the 'e' series samples in order to preserve the gouge structure upon unloading and removal from the shearing apparatus. Because this clamp may have contributed a slight amount of friction during the run, the friction data from these samples were considered unreliable and were not analyzed. All the above experiments were conducted at a normal stress of 10 MPa. A third set of three runs was performed at the higher normal stress of 25 MPa. They were otherwise similar to R1-710 runs at 10 MPa and are therefore labeled R1-710 (25 MPa). A fourth set of four runs was made at 10 MPa normal stress in which the gouge was prepared from the single size fraction

Table 1. Experimental conditions

Run	Roughness No.	Thickness (mm)	Size cutoff (mm)	Shear (μm)
Series R1 (rough surface; 1 mm gouge)				
R1-45	60	1	45	10,000
R1-90	60	1	90	10,000
R1-180	60	1	180	10,000
R1-360	60	1	360	10,000
R1-710a	60	1	710	10,000
R1-710b	60	1	710	10,000
R1-710c	60	1	710	10,000
Series R3 (rough surface; 3 mm gouge)				
R3-45	60	3	45	10,000
R3-90	60	3	90	10,000
R3-180a	60	3	180	10,000
R3-180b	60	3	180	10,000
R3-180c	60	3	180	10,000
R3-360	60	3	360	10,000
R3-710a	60	3	710	10,000
R3-710b	60	3	710	10,000
R3-710c	60	3	710	15,000
R3-710d	60	3	710	15,000
R3-710e	60	3	710	15,000
Series S3 (smooth surface; 3 mm gouge)				
S3-45	600	3	45	10,000
S3-90	600	3	45	10,000
S3-180a	600	3	180	10,000
S3-180b	600	3	180	10,000
S3-180c	600	3	180	10,000
S3-710a	600	3	710	10,000
S3-710b	600	3	710	10,000
S3-710c	600	3	710	10,000
R3-All 710 (rough surface; 3 mm gouge)*				
All 710	60	3	All 710	10,000

* The gouge for this run was composed of particles with diameters between 360 and 710 μm only.

between 360 and 710 μm diameter. The objectives were (1) to test the hypothesis (Sammis *et al.* 1987) that the constrained comminution of a non-fractal gouge should produce a fractal one, and (2) to observe the evolution of frictional parameters during comminution and compare them with those observed for initially fractal gouges. One run was made to obtain frictional data and the other three runs were epoxy impregnated. These were denoted as R3-All 710 and R_e3-All 710.

Each three-block assembly was placed in the apparatus and the normal load applied with the horizontal ram. The servo-controller then advanced the vertical ram at the prescribed rate following the cyclic velocity-stepping program. At the end of each run the vertical ram was withdrawn first, followed by the horizontal. The entire sample block sandwich was retrieved from the apparatus and carefully disassembled for inspection of the gouge and surfaces. In the case of the 'e' series samples, the vertical (shear) load was removed and then the clamp was closed around the sample before the horizontal (normal) load was withdrawn. The clamped three-block sandwich, with gouge intact, was then completely vacuum impregnated with a low-viscosity epoxy.

EXPERIMENTAL RESULTS

Microscopic observations of the epoxy-impregnated gouge layers will be discussed first. Mechanical data will then be presented and discussed.

Thin-section observations.

The vacuum-impregnated sample assemblies were sectioned in the plane containing the simple shear strain and thin sections were prepared. Photomicrographs were taken in reflected light and assembled into photomosaics. Samples which began with a uniform particle size distribution and were designed to test the nearest-neighbor comminution model are discussed first. Then those experiments which began with a self-similar fractal grain size distribution will be discussed.

Evolution of an initially uniform particle distribution: the R_e3-all 710 μm-series

Three sample assemblies were prepared with a 3 mm thick gouge layer having a uniform particle size distri-

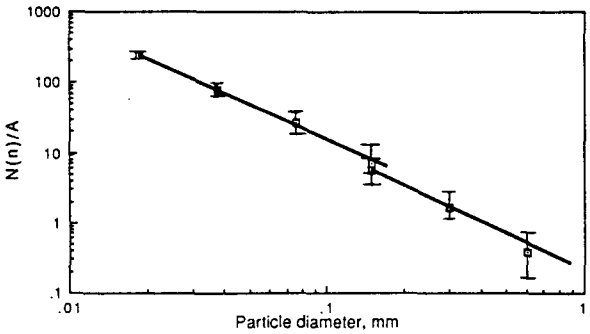

Fig. 3. Particle density as a function of grain size for the R_e 3-All 710 after 10.0 mm slip. Data for the three largest grain sizes were taken from Fig. 4(c). Data for the four smallest sizes were taken from another photomosaic at ×400 magnification. The two counts overlap at 180 μm grain diameter. The slopes are consistent, the slight offset is not significant.

bution between 360 and 710 μm in diameter. The samples were sheared to displacements of 1.0, 5.5 and 10.0 mm. Epoxy-impregnated thin sections are shown in Fig. 4. After a displacement of 1.0 mm, significant comminution had already taken place (Fig. 4a), with many of the largest grains being reduced to smaller sizes. Note that many of the particles appear to have failed in tension, presumably by loading under compression, as hypothesized by Sammis *et al.* (1987). As predicted by elasticity theory (Timoshenko & Goodier 1951), many particles show tensile cracks radiating from poles of compression. The smaller particles formed from these radial cracks contribute to the high percentage of smaller particles in the gouge layer. The intergranular porosity is still quite large. Figure 4(b) shows the gouge layer after 5.5 mm of slip. Very few particles have nearest neighbors the same size, and the void space has been greatly reduced. A layer of smaller particles is observed near the gouge–rock surface; the homogeneity of comminution appears to break down near this interface. Figure 4(c) shows the gouge layer after 10 mm of displacement. The porosity has been further reduced, as well as the density of the largest grains.

Figure 3 shows the particle density as a function of diameter from 10 to 710 μm. A transparent overlay of concentric circles, each differing in diameter by a factor of 2, was used to sort the grains into binary size classes denoted n. The mean diameter of particles in class n is thus twice that of particles in class $n + 1$. The number of particles of class n counted in an area A of the photomosaic is denoted $N(n)$. The full counting procedure is detailed in Sammis *et al.* (1987). The linear dependence of log of the particle density ($N(n)/A$) on the log of the particle diameter in Fig. 3 shows that the gouge has a self-similar particle distribution over the range examined. The small offset is due to a change in photomosaics at higher magnification and is not significant. The slope yields a fractal dimension of 2.6 with a maximum variation of about 0.3. This is the same dimension observed by Sammis *et al.* (1987) for a natural fault gouge, and is also the value predicted by the nearest neighbor comminution micromechanism. In fact, a comparison of Fig. 4 with the natural fault gouge shown in Figs. 2–9 in Sammis *et al.* (1987) supports the hypothesis that the same comminution and deformation mechanisms are operating in these laboratory faults as in natural crustal faults.

The structure of fractal gouge layers: the R_e3- and S_e3-series

The gouge layers from R_e3-45, -180 and -710 and those from S_e3-45, -180 and -710, are exhibited in Figs. 5–8. In Fig. 5 the upper block has moved to the left relative to the lower block. In Figs. 6–8 the upper block has moved to the right relative to the lower block. Note that the original self-similar grain distribution appears to remain more or less well preserved to the end of the run. However, a comparison of particle counts on R_e3-710 and S_e3-710, and R_e3-180 and S_e3-180 (Figs. 9a & b, respectively), shows important differences. While the densities of the largest grains for both the rough and smooth surfaces are equal, the densities of the next two smaller classes of grains are different. In Fig. 9(a), the experiments with smooth surfaces have more grains in the smaller class than those with rough surfaces. Because the initial grain distribution was the same for each pair, any difference in particle density must be a result of the shear strain. The observed difference may be interpreted as being due to the removal of the smaller fractions in the case of the rough surface by comminution to fractions even smaller than those measured. In the case of smooth surfaces, grains from the largest class fracture and add to the observed smaller classes, but then grains are not removed to even smaller classes by further comminution. In Fig. 9(b) this crossover occurs at a larger grain-size. The observation that rough surfaces produce more comminution is important to the micromechanical model developed below.

Figures 5–8 also support the 'nearest neighbor' rule proposed by Sammis *et al.* (1987). No two particles of the same size are observed next to each other without one of them undergoing fracture. Only one instance of a breakdown of the nearest neighbor rule can be found in the thin sections. Bands are observed within the R3-45 and -180 samples that are oriented between 15 and 25° to the gouge–rock interface. These bands, which resemble Reidel shears (Morgenstern & Tchalenko 1967, Tchalenko 1968, 1970), are between 100 and 200 μm wide. Close inspection reveals that, within these bands, the density of smaller grains exceeds that of the surrounding gouge and nearest neighbors the same size are commonly observed. This observation is consistent with experiments in which Ottawa sand, sheared to several millimeters displacement under triaxial conditions, produced fault gouge with a fractal dimension approaching 2.6, except within narrow bands oriented similar to Reidel shears where the fractal dimension approaches 3.0 (Scholz personal communication).

The figures also reveal that the surface roughness is not significantly changed during shear displacement in the R_e3-series. Note that incipient spalling of the sliding blocks is evident in some of the figures, but there is very

little change in surface roughness between a sample sheared 2.5 mm and one sheared 10 mm.

The R_e3-45 and S_e3-45 samples show an interesting set of features. Figure 5 shows elongate pores within R_e3-45, many of them more than 1 mm long and with apertures 10–30 μm across. Some of these pores lie parallel and adjacent to the gouge–rock surface. Many more traverse the gouge layer at an angle of 10–30° to the gouge–rock surface, lying within or sub-parallel to the bands described above. S_e3-45 also contains elongate pores both along the gouge–rock surface and extending through the gouge layer at an angle between 10 and 30° to the interface (Fig. 5). These pores are only a fraction of the length of the pores in R_e3-45, but they have apertures several times their widths. Although we offer no obvious explanation for these features, they have been observed by other investigators (Logan & Scholz personal communications).

MECHANICAL DATA

The R1-, R3- and S3-series of experiments were conducted to measure four friction parameters: (1) the coefficient of friction, μ; (2) the instantaneous velocity response, or a-value; (3) the transient relaxation, or b-value; and (4) the characteristic displacement, D_c. The coefficient of friction, μ, was monitored throughout the course of the experiments. The three transient parameters, a, b and D_c, were measured for each step change in the sliding velocity (see Fig. 1).

As discussed above, the a-value quantifies the instantaneous change in the friction coefficient in response to a step-change in the velocity. If a velocity increase (or decrease) causes a corresponding instantaneous increase (or decrease) in the friction coefficient from an initial value, μ_i, to a peak value, μ_p, then the a-value is defined as

$$a = |\mu_i - \mu_p|. \tag{4}$$

As displacement proceeds after the velocity change, the coefficient of friction relaxes to a residual value, μ_r, over a displacement proportional to the characteristic displacement, D_c. The magnitude of the relaxation is denoted by b, where

$$b = |\mu_p - \mu_r|. \tag{5}$$

If $b \neq a$, then the residual value of friction coefficient will not be equal to the initial value before the velocity change. Whenever $b < a$, the system is said to exhibit velocity strengthening, meaning that a velocity increase raises the coefficient of friction. If $b > a$, the system is said to velocity weaken. This decrease in μ with increasing velocity is a necessary, but not sufficient, condition for a stick–slip instability. Velocity dependence is often characterized by $a - b$. If $a - b > 0$, the system velocity strengthens, if $a - b < 0$, the system velocity weakens.

Following a step change in velocity, a displacement proportional to the characteristic displacement D_c is required for a new equilibrium value of friction, μ_r, to be reached. The characteristic displacement was obtained by fitting the equation

$$\mu(x) = \mu_r + \mu_p \exp\{-d/D\}_c, \tag{6}$$

where d is the shear slip following the velocity change. The parameters a, b and D_c were recorded at each velocity change. Changes in the gouge layer thickness, h, were also recorded throughout the experiment.

Six experimental variables were changed during the R1-, R3- and S3-series of experiments to test their effect on the friction parameters. These variables were: (1) the total displacement; (2) the velocity (1 and 10 μm s^{-1}); (3) the normal stress (10 and 25 MPa); (4) the upper particle cutoff (45, 90, 180, 360 and 710 μm); (5) the surface roughness (rough = No. 60 grit, and smooth = No. 600 grit); and (6) the layer thickness (1 and 3 mm). Velocity and normal stress were controlled throughout the experiment by the high-speed servo-controller. The other three variables, upper particle cutoff, surface roughness and layer thickness were given initial values at the start of each run, but then allowed to freely evolve as the experiment proceeded.

Experimental uncertainty in the friction parameters was estimated by repeating some runs several times (see Table 1). Standard deviations thus found are included on all experimental plots to aid in assessing the significance of any differences noted.

The coefficient of friction, μ

The coefficient of friction is plotted as a function of displacement for the different upper particle cutoffs in Fig. 10. These data are summarized in Fig. 11, which shows the value of μ after 10 mm of displacement as a function of the maximum particle size for the three series. Several general trends are apparent. There is an obvious effect of layer thickness for the case of rough surfaces. The 1 mm thick layer has a significantly higher coefficient of friction than the 3 mm thick layer. There is also an obvious effect of surface roughness. The smooth surfaces have a significantly lower μ than the rough surfaces for all particle sizes. Another difference between rough and smooth surfaces is that μ tends to decrease with increasing upper fractal cutoff for the rough surfaces while μ for the smooth surfaces is independent of the upper cutoff size.

These observations place important constraints on models for the micromechanics of friction in gouge layers. The consistent difference between the R1 and R3 layers rules out the possibility that the difference between rough and smooth surfaces is a surface effect which does not extend through the bulk of the gouge. Moreover, the difference in μ between R1 and R3 configurations cannot be due to the 3× higher strain rate in the R1 layer. Velocity stepping during each run produces a 10× increase in strain rate, but less than a 1% change in μ.

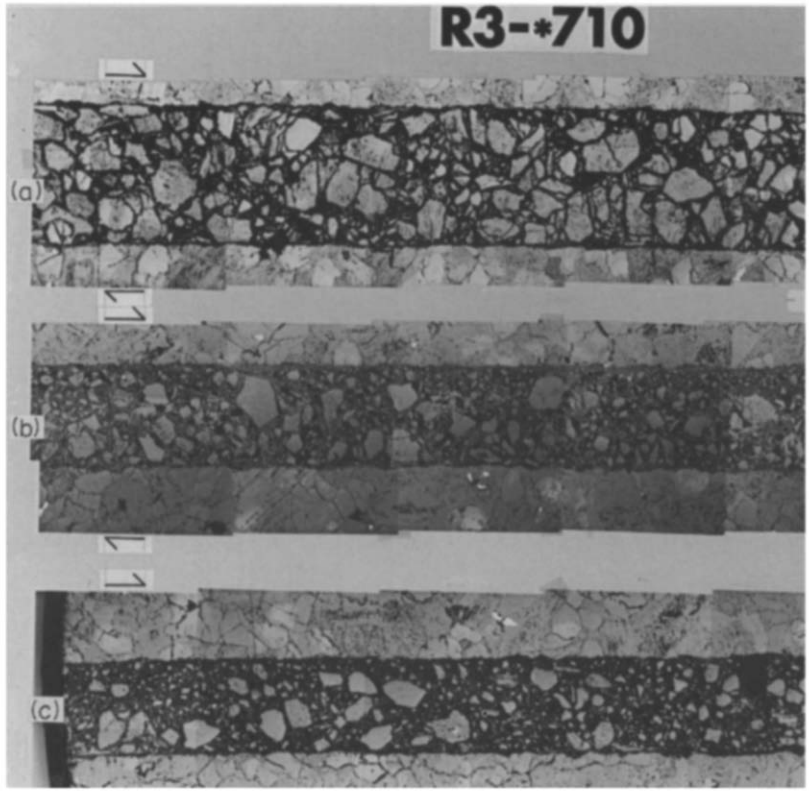

Fig. 4. Optical photomosaics of R_e3-All 710 at a magnification ×50. The upper block has moved to the right relative to the lower block in each case. Mosaic (a) was prepared after 1.0 mm slip. Notice grains fracturing under tension from loading at poles. Also note large volume of void space. Mosaic (b) shows a layer after 5.5 mm of slip. The void space has been greatly reduced and no grains can be seen with nearest neighbors the same size. Mosaic (c) shows a layer after 10.0 mm of slip. The gouge now has a self-similar grain size distribution with a three-dimensional fractal dimension of about 2.6. Notice how the self-similar distribution has reduced void space in sample. Also note that the surface roughness has remained similar to roughness near the start of the run in mosaic (a).

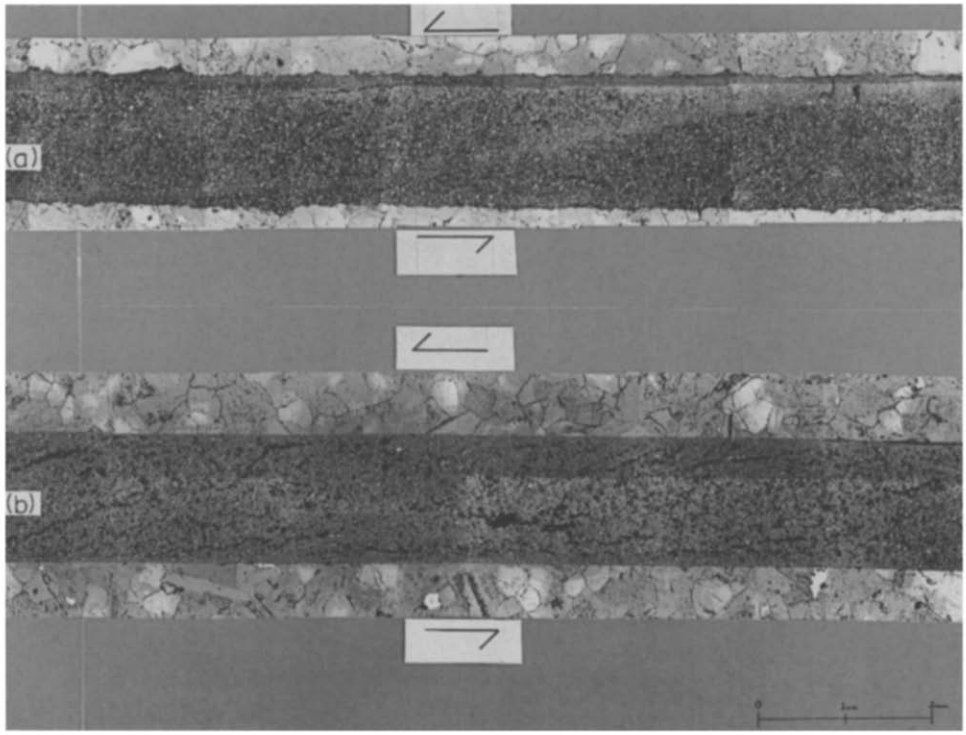

Fig. 5. Optical photomosaics of (a) R_e3-45 and (b) S_e3-45 at magnifications ×50 after 10 mm of shear displacement. In (a) note the bands of denser material traversing the gouge at an angle between 6 and 10° from the gouge–rock interface, and the elongate pores along the gouge–rock interface. In (b) note the elongate pores crossing the gouge at oblique angles to the gouge–rock surface.

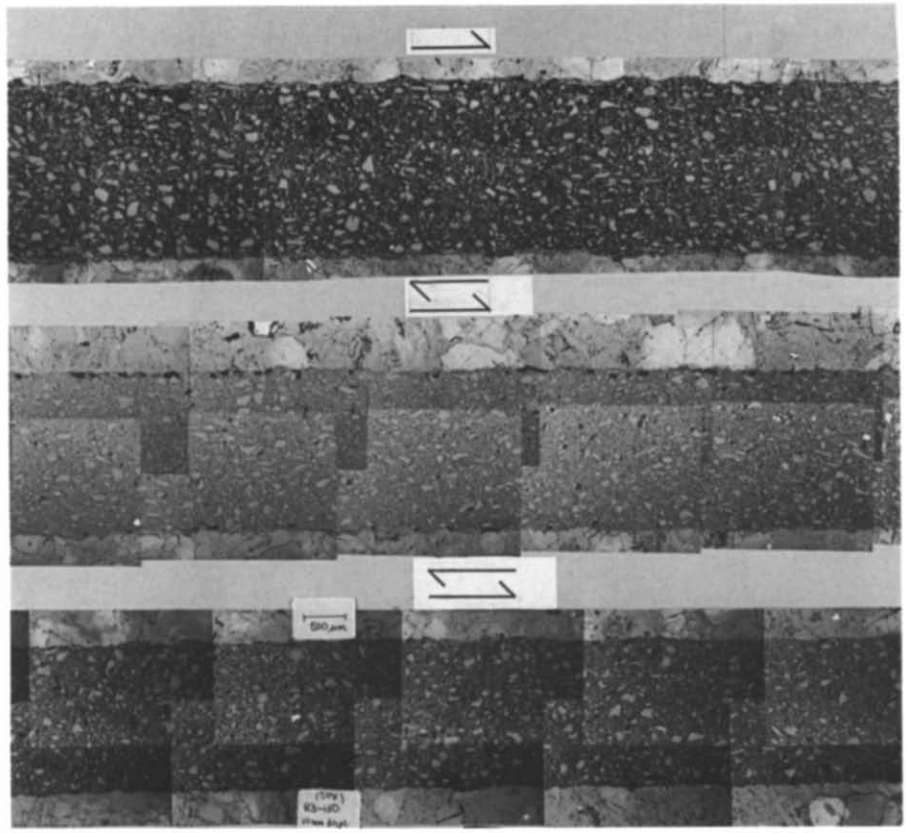

Fig. 6. Optical photomosaics of R_e3-180 at a magnification of ×50. Upper, center and lower mosaics represent samples sheared 2.5, 5.5 and 10.0 mm, respectively. Notice surface roughness remains about the same in all three samples.

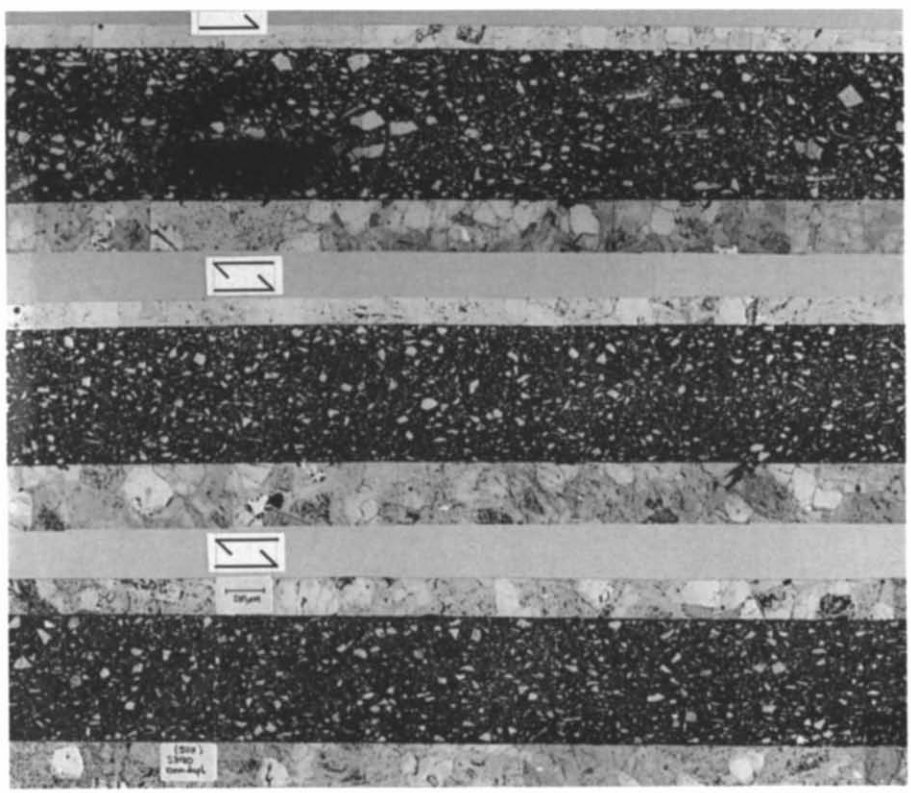

Fig. 7. Optical photomosaic of S_e3-180 at magnification ×50. Upper, center and lower mosaics represent samples sheared 2.5, 5.5 and 10.0 mm, respectively.

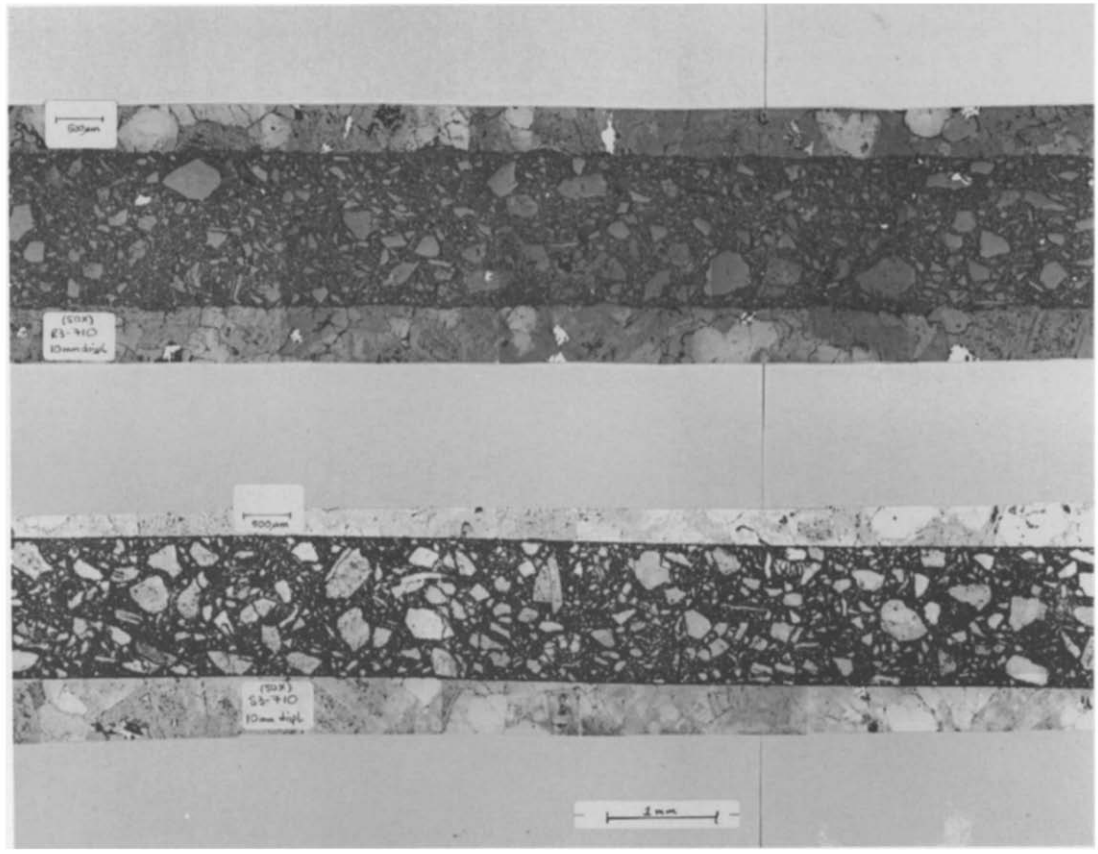

Fig. 8. Optical photomosaics of R_c3-710 and S_c3-710 at a magnification of ×50 after 10 mm of slip. Notice the homogeneous distribution of largest grains with no nearest neighbors the same size.

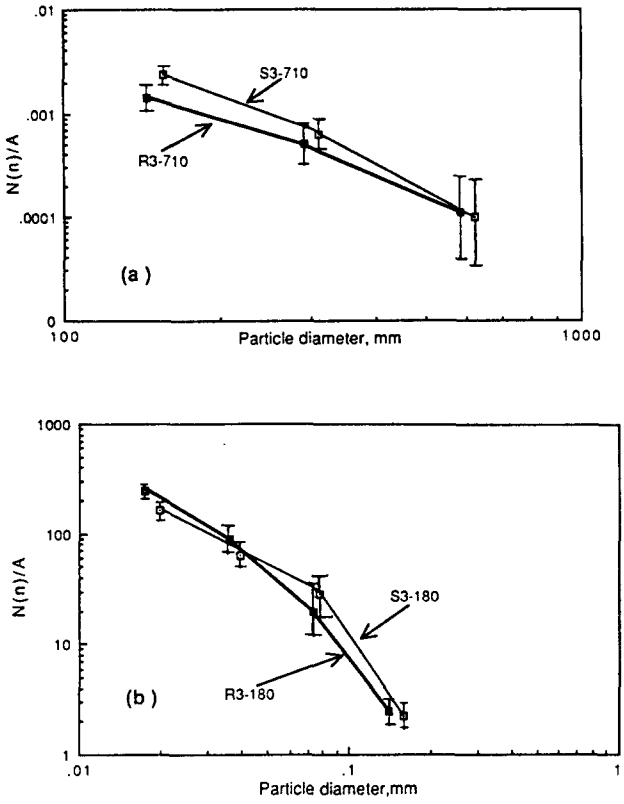

Fig. 9. (a) Particle density as a function of particle diameter for R_e3-710 and S_e3-710. Note the difference in density between rough and smooth samples for particles 180–360 mm and 90–180 mm in diameter. Note also that the largest particles have the same density. (b) Particle density as a function of particle diameter for R_e3-180 and S_e3-180. Note the different densities for the smaller particles.

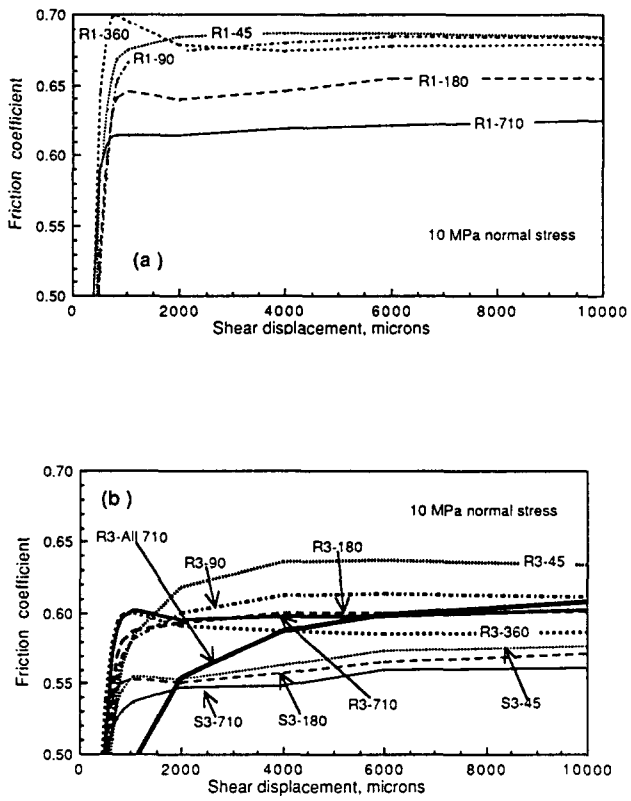

Fig. 10. Friction coefficient as a function of displacement (a) for the R1-series and (b) for the R3- and S3-series.

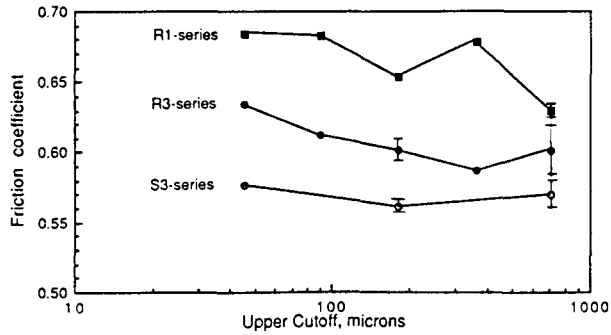

Fig. 11. Friction coefficient after 10 mm of displacement as a function of the upper fractal cutoff diameter for the R1-, R3- and S3-series.

The instantaneous velocity response: a-*value*

Figure 12 shows the *a*-value as a function of displacement for different upper particle cutoffs. Values for velocity increase are plotted separately from velocity decrease. The *a*-value does not appear to be sensitive to the upper cutoff diameter or the normal stress. The figures also illustrate that the *a*-value decreases as a function of displacement, with the largest changes occurring within the first 1.0 mm of the run. This change is most noticeable for the S3-series (Fig. 12c) in which the *a*-value decreases from about 0.02 to 0.01 with the first millimeter of slip. The *a*-value is most sensitive to surface roughness (Figs. 12c & d). The *a*-value for the smooth surfaces is only about one third that for the rough surfaces.

The relaxation parameter: b-*value*

Figure 13 shows the *b*-value as a function of slip distance for all the upper particle cutoffs. Like the *a*-values, the *b*-values are plotted separately for velocity increase and decrease.

The most significant differences in the *b*-values are associated with differences in surface roughness (Figs. 13c & d). The *b*-values for rough and smooth surfaces start almost equal, but then diverge soon after slip begins. The smooth surfaces maintain a nearly constant *b*-value while the *b*-value for rough surfaces increases, especially at the start of the run. It is this displacement-dependent increase in *b*-value which is responsible for the decrease of velocity strengthening in all rough samples and the onset of velocity weakening (recall that the *a*-value remains almost constant after about 1.0 mm slip in all cases).

The velocity dependence: a − b

The velocity dependence is plotted for the R1-, R3- and S3-series in Fig. 14. Values for a velocity increase are plotted separately from those for a velocity decrease. The smooth samples show significant velocity weakening after a very small amount of displacement, and this weakening does not change significantly throughout the remainder of the experiment. For the rough samples,

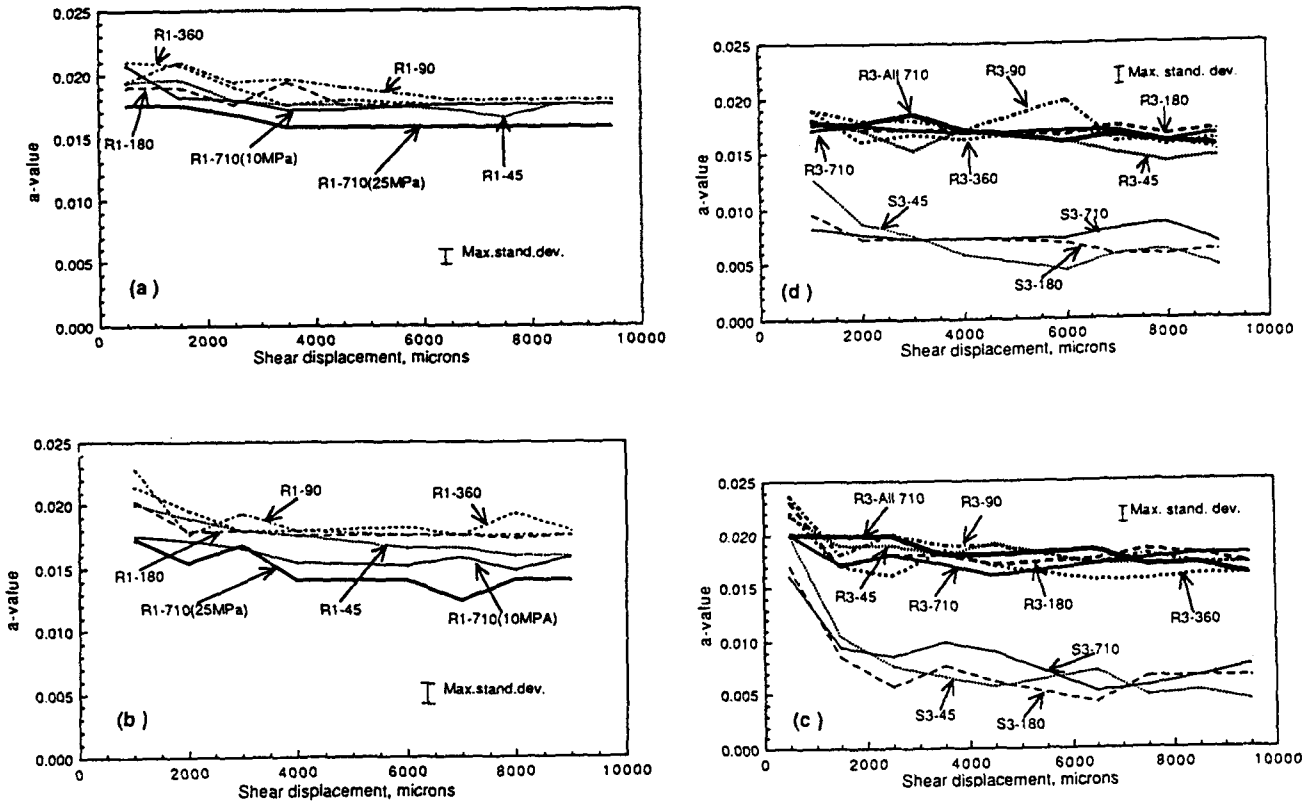

Fig. 12. The a-value as a function of displacement: (a) for a velocity increase for the R1-series; (b) for a velocity decrease for the R1-series; (c) for a velocity increase for the R3- and S3-series; and (d) for a velocity decrease for the R3- and S3-series.

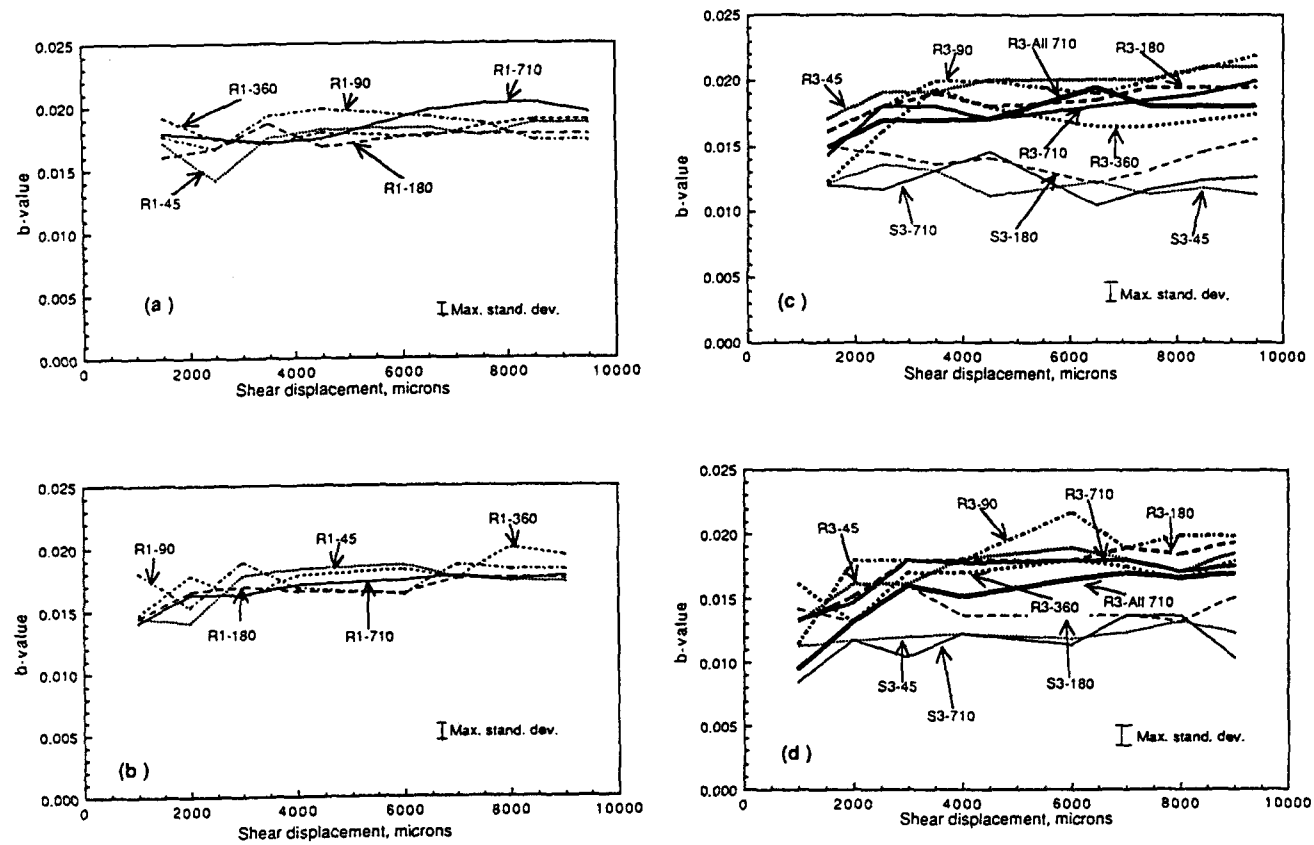

Fig. 13. The b-value as a function of displacement: (a) following a velocity increase for the R1-series; (b) following a velocity decrease for the R1-series; (c) following a velocity increase for the R3- and S3-series; and (d) following a velocity decrease for the R3- and S3-series.

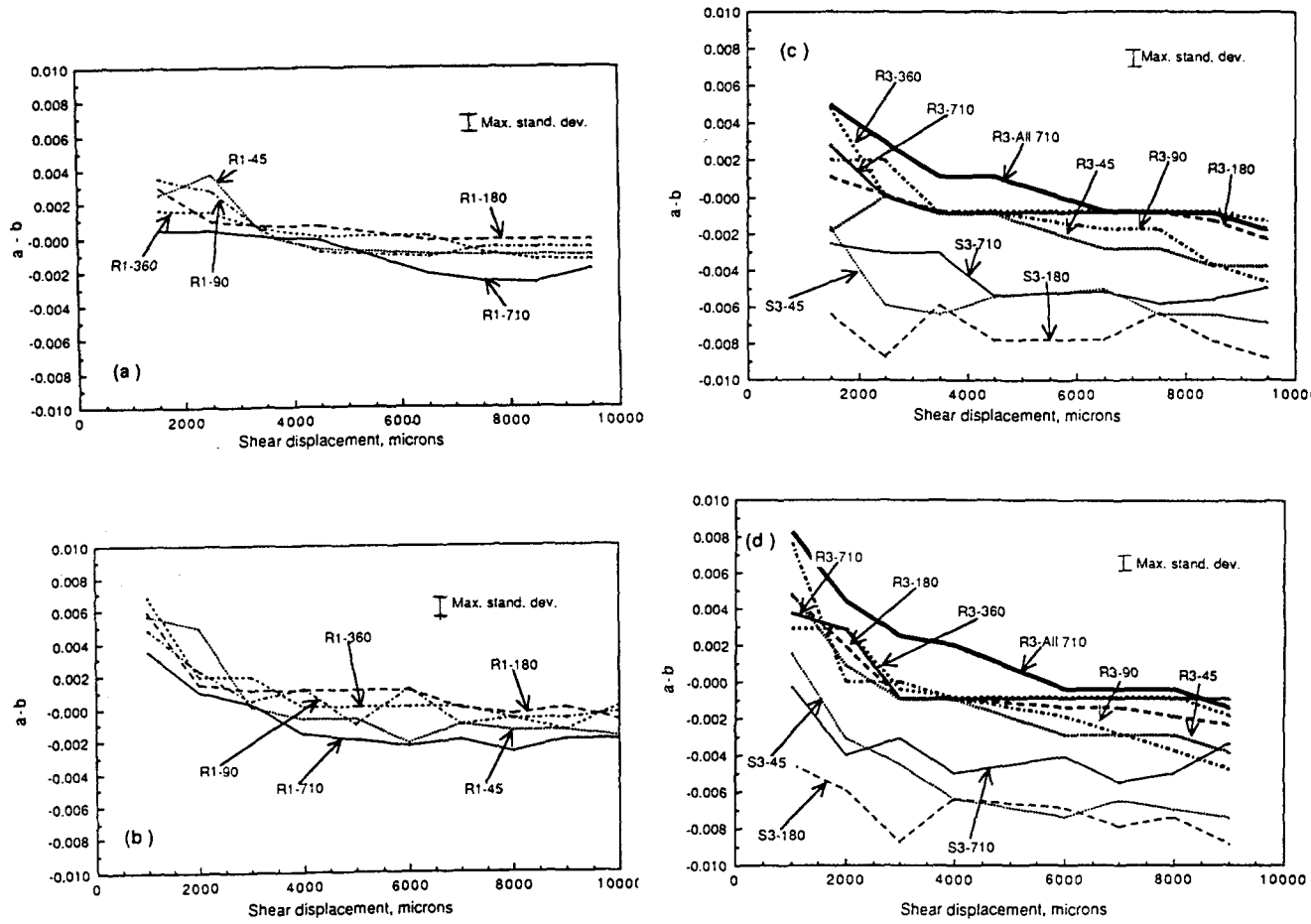

Fig. 14. Parameter $a - b$ as a function of displacement: (a) following a velocity increase for the R1-series; (b) following a velocity decrease for the R1-series; (c) following a velocity increase for the R3- and S3-series; and (d) following a velocity decrease as a function of displacement for the R3- and S3-series.

$a - b$ is always positive at the start of the experiment and decreases with increasing displacement, but the rate of decrease diminishes with slip. For both the R1- and R3-series, all upper particle cutoffs show velocity weakening at the end of the run. Note that R3-All 710 gouge velocity-strengthened throughout the first 6.0 mm of the run, but then weakened to achieve a velocity dependence of -0.0015 after 10 mm of shear displacement, comparable to that of the initially fractal R3-710.

The average value of $a - b$ for five runs of R3-710 is approximately zero, but the R3-45 sample achieved a large negative value of $a - b$ nearly equal to that of the smooth samples. These data suggest that two mechanisms are capable of producing negative velocity dependence, one which functions in the presence of an initially 'smooth' surface (S3-series), and one that operates in 'rough' surface environments (R3-series) in which the gouge structure has been sufficiently changed by shear displacement. While it is tempting to conclude that the rough samples simply evolve into smooth samples by either polishing the surfaces or filling in the roughness with small particles, this interpretation is not supported by the thin sections. Other mechanical observations also argue against this evolution from rough to smooth. The values of μ, a and b for rough surfaces do not approach those of smooth surfaces with increased displacement over the range of displacements we studied.

Figure 15 shows the effect of normal stress on $a - b$. Although the R1-710 (25 MPa) initially show greater velocity strengthening, this difference disappears with increasing displacement. After 10 mm of slip R1-710 (25 MPa) has the same value of $a - b$ as R1-710 (10 MPa).

The characteristic displacement: D_c

The characteristic displacement tends to decrease throughout the experiment. In Fig. 16(a), D_c for the R1-series falls from a value between 30 and 50 μm, to a value between 10 and 20 μm. For the R3-series (Fig. 16b), D_c decreases from between 50 and 80 μm to a value between 15 and 40 μm. For the S3-series (Fig. 16b), D_c is almost constant from the start of the run to the finish. Only a slight decrease is apparent by the end, from between 15 and 30 μm to between 5 and 15 μm.

There is no strong dependence of D_c on the upper particle cutoff, as proposed by Sammis & Biegel (1989), although a weak relation is suggested by the R1-45 and R3-45 data. The D_c for these fine gouges is consistently less than that for the coarser gouges by the end of the run. Finally, note that the characteristic displacement for R3-All 710 increases for the first 3 mm displacement to a value twice that of the other gouges (about 130 μm) but then decreases to a final value of 40 μm by the end of the run.

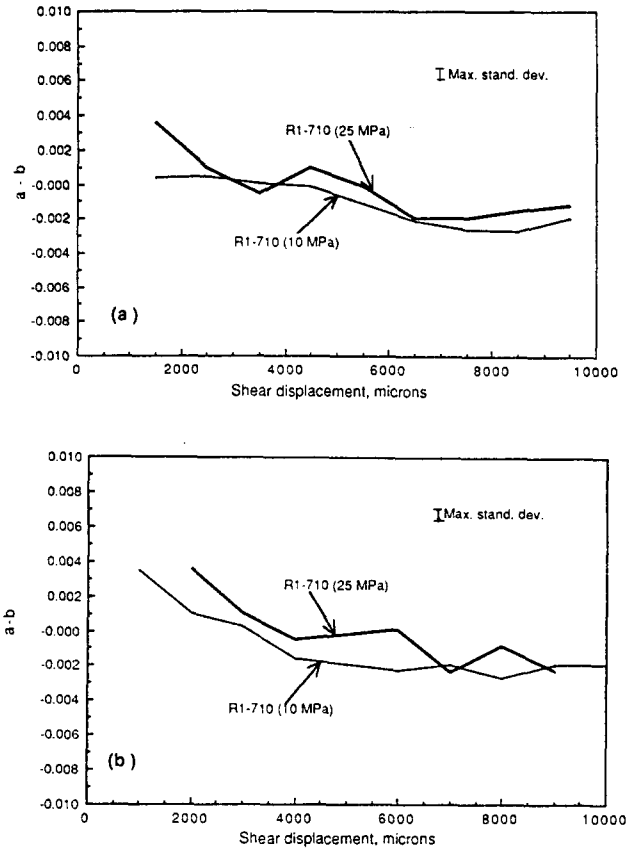

Fig. 15. Parameter $a - b$ as a function of displacement for R1-710 at a normal stress of 10 and 25 MPa: (a) following a velocity increase; and (b) following a velocity decrease.

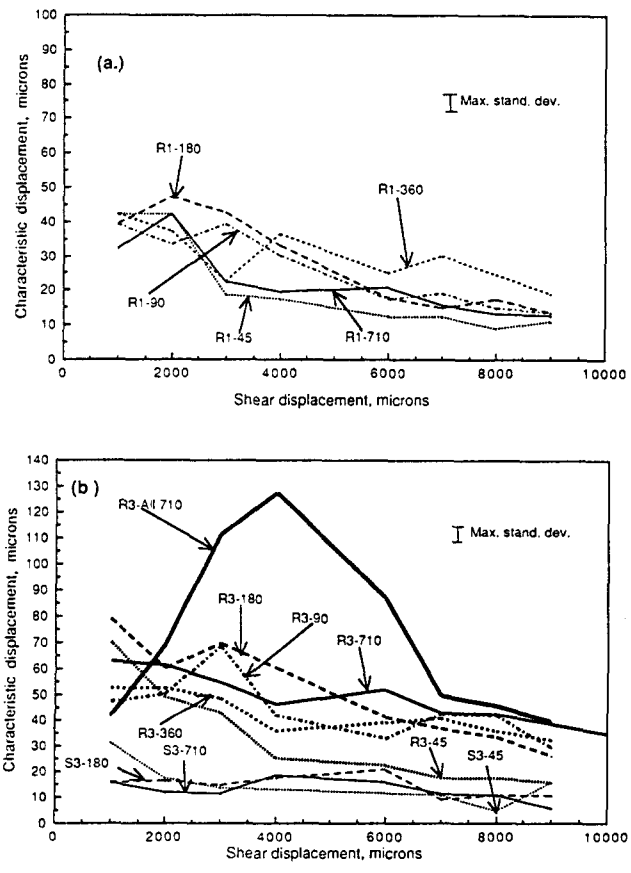

Fig. 16. Characteristic displacement D_c as a function of total displacement: (a) for the R1-series; and (b) for the R3- and S3-series.

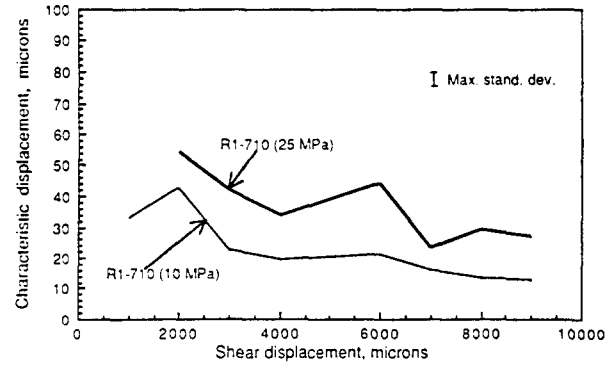

Fig. 17. Characteristic displacement D_c as a function of total displacement for R1-710 at a normal stress of 10 and 25 MPa.

Layer thickness also has a weak effect on the characteristic displacement. While no obvious trend is apparent, the characteristic displacement for the R3-series is slightly greater than that for the R1-series.

The initial characteristic displacement is sensitive to the surface roughness, but this difference almost disappears by the end of the run. Figure 16(b) compares D_c for the R3- and S3-series. Although D_c for R3-45 and R3-710 are nearly identical at the beginning of the run, by the end the R3-45 gouge D_c has evolved to a value approximately equal to that of the S3-series, while D_c for R3-710 is more than twice as large.

Normal stress also influences the characteristic displacement. Figure 17 compares D_c for R1-710 at 10 MPa normal stress with that at 25 MPa. It shows that D_c for the 25 MPa run has values nearly twice that of the 10 MPa run for similar slip distances. This observation suggests that D_c is related to the size of the adhesive contact between particles rather than to the particle geometry. The decrease in D_c observed in the case of rough surfaces may be due to the evolution of a more homogeneous stress distribution in which the applied load is carried by more particle contacts. Similarly, the initial increase in D_c for R3-All 710 may indicate the formation of a more heterogeneous stress state in which a smaller number of structures in the gouge carry the load. By the end of the R3-All 710 run, a self-similar particle distribution has been established (Fig. 3), the load is more uniformly distributed, and D_c falls to a more typical value.

Compaction: δh

The change in gouge layer thickness is continuously measured by a displacement transducer on the horizontal ram. Figure 18 shows the change in thickness measured from the start of the run as a function of displacement for each of the different particle size cutoffs. The absolute value of the gouge thickness was determined by measuring the thickness of the gouge in the R_e3- and S_e3-series thin sections at the end of the run. Using the measured change in thickness, the 3 mm layer is estimated to have been 2.2 mm thick after compaction by the normal load but before any shear displacement. Assuming the compaction of the 1 mm

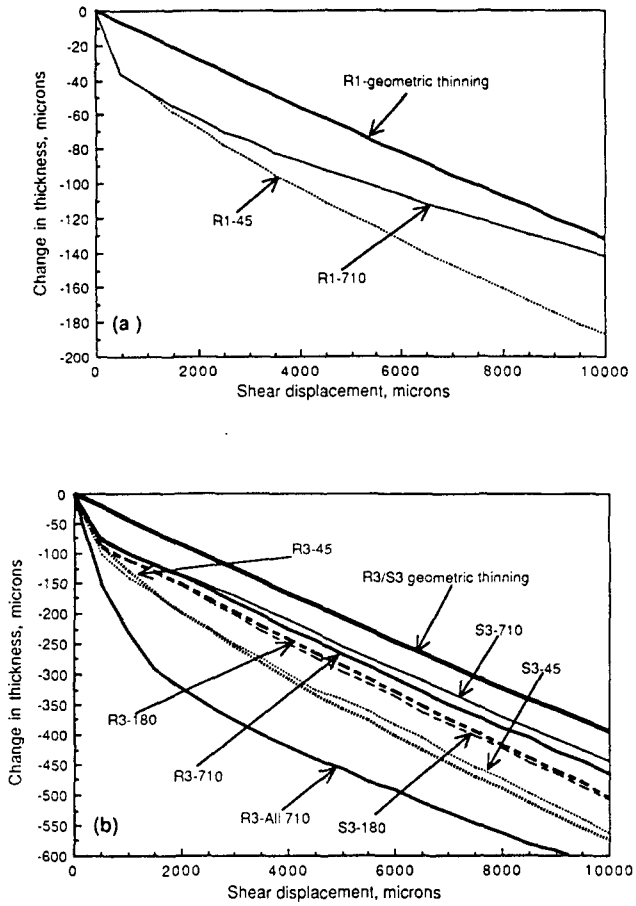

Fig. 18. Compaction of gouge layers as a function of displacement. Geometric thinning curve shows the expected decrease in layer thickness due to gouge loss from the bottom of the sliding block. Plot (a) is for the R1-series, (b) is for the R3- and S3-series.

layer is proportional to that of the 3 mm layer, then the R1-series gouge was about 700 μm thick at the onset of shear displacement. This is equal to the diameter of the largest grains in the R1-710 gouge and may explain the anomalous frictional behaviour observed in these runs (Fig. 10a).

Figure 18 also shows the 'geometric thinning' expected for these samples. If the gouge deforms only by shear without internal dilatation or compaction, the layer is still expected to become thinner as the shear displacement causes gouge to fall out of the bottom of the vertical sandwich without being replaced at the top. The conservation of gouge volume yields a simple relation between instantaneous gouge thickness h and displacement x:

$$dh = (h/L)\,dx, \tag{7}$$

where L is the length of the sliding block.

Figure 18(b) shows that there is no significant difference between compaction curves for the rough and smooth samples. This finding is supported by the thin sections (R_e3- and S_e3-series) which show nearly identical thicknesses for both surfaces throughout the run. No dilatancy was detected in any of the samples, except R1-710 (Fig. 18a) which may be associated with the largest grain diameter approaching the layer thickness. Failure to record dilatancy, however, may be due to the limited resolution of our equipment, and does not preclude dilatancy on the order of several microns.

A trend is evident for gouge with smaller size cutoffs to exhibit greater compaction. Note, however, that nearly all compaction occurs within the first 1 mm of slip, after which there is no noticeable difference. The exception is the R3-All 710 which compacts over at least the first 2 mm of slip.

THE MICROMECHANICS OF GOUGE DEFORMATION

The motion of the sliding blocks in the double-shear friction experiments described above is accommodated by a combination of four possible mechanisms within the gouge layer: (1) fracture of the particles; (2) frictional slip between the particles; (3) frictional slip of the particles along the surfaces of the sliding blocks; and (4) fracture of the surface of the sliding blocks (wear). The value of the coefficient of friction and of its transient parameters depend upon the relative importance of these four mechanisms under a given set of experimental conditions. If slip between particles or along the interface is dominant, then the usual micromechanical models for the fracturing of asperities whose strength depends upon their average lifetime are appropriate, and velocity weakening and stick–slip instability are possible. If, on the other hand, gouge deformation is dominated by fracture of the particles or by spalling of the sliding surfaces, then the fracture strength does not increase with time and the frictional behavior of the layer should be characterized by velocity strengthening.

The partitioning of the deformation between fracture and slip may be expected to depend on experimental variables such as the normal stress, the particle size distribution, the layer thickness, the surface roughness of the sliding blocks, and even the sliding velocity. In order to assess the relative importance of fracture and slip for a given set of experimental conditions, we first need to assess the state of stress in a granular layer deforming in simple shear.

The state of stress within a gouge layer

The double-shear apparatus applies a known normal and shear stress to the boundaries of the gouge layer, but this is not sufficient to determine the state of stress within the layer (it only gives a single point on the Mohr stress diagram). Mandl *et al.* (1977) measured the stress orientation within a granular mass undergoing simple shear at a constant boundary velocity. They found that the principal stress σ_1 was inclined at 45° ± 2° to the interface such that all planes parallel to the boundary are planes of maximum shear. This was true for dilating layers at low normal stress as well as for layers in which the normal stress was large enough to suppress dilatation by extensive grain crushing.

Mandl *et al.* (1977) also found evidence that the state

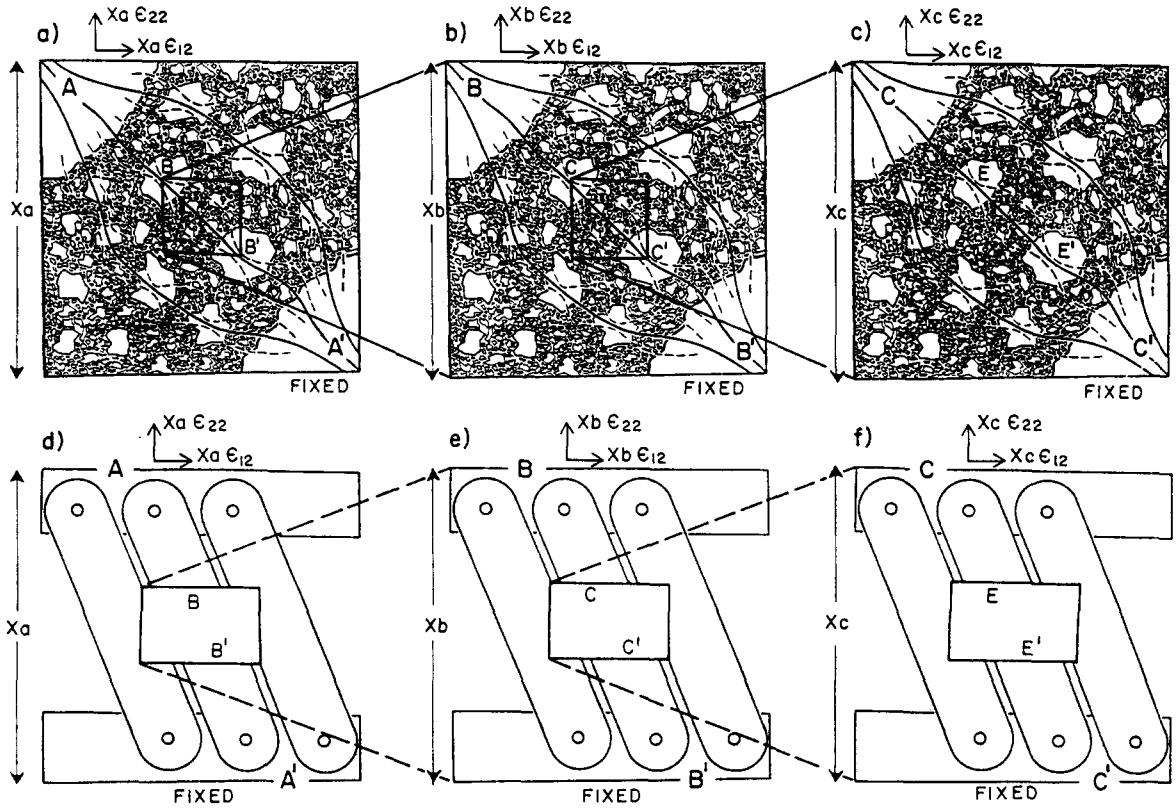

Fig. 19. Hypothetical network of stress paths in a fractal gouge. Parts (a), (b) and (c) demonstrate how each stress path is composed of a hierarchy of stress paths at smaller scales. In (d), (e) and (f), stress paths are idealized as beams demonstrating how simple shear places the particles in longitudinal compression. (After Sammis *et al.* 1987.)

of stress within the layer is not homogeneous. They reported observing the "continual and changing formation of grain 'bridges'" in their transparent rotary apparatus. They also observed large fluctuations in the magnitude of the stress at a given point within the gouge that are probably associated with the formation and destruction of such load-bearing bridges. Further evidence for load-bearing structures within gouge comes from two-dimensional photoelastic studies of granular masses (Gallagher *et al.* 1974, Oda & Konishi 1974, Allersma 1982, Oda *et al.* 1982) where it has been observed that critical load-bearing contacts (and associated microfractures) tend to join together in series or chains.

Our model for the micromechanics of friction in a gouge layer will therefore be built upon the assumption that the state of stress within a granular layer being deformed in simple shear is heterogeneous, with the applied normal and shear stresses being supported by a finite number of grain bridges which span the layer. Particles between bridges do not bear the load and are free to move as required to accommodate motion of the bridges. Figure 19 shows how such stress-bearing bridges might be envisioned in a self-similar gouge, and how they might be approximated as rotating beams. Rotation of a bridge increases the stress which it supports until it fails and the stress is supported by other, newly formed bridges.

In this model, the frictional behavior of a granular layer depends upon the failure mode of its load-bearing bridges. If most bridges fail by sliding, either between particles or at the interface, then adhesion is involved and the usual mechanisms which produce velocity weakening apply (Dieterich 1979a, Tullis & Weeks 1986). For example, when the velocity is increased, the resulting increase in the fracture strength of adhesions due to the higher loading-rate is compensated by the decrease in their strength associated with the decrease in their average lifetime. If, on the other hand, most bridges fail by fracture of the particles or spalling of the wallrock, then velocity strengthening is to be expected. This is because the fracture strength is higher at the higher loading rates associated with faster sliding velocities, and there is no compensating time dependence of the strength.

The failure mode of a load-bearing bridge

A grain bridge can fail in any of the four modes illustrated in Fig. 20. These are the crushing of the particles, slip between the particles, slip between particles and the surface of the sliding block, and failure of the surface of the sliding block which spalls new material into the gouge layer. We now wish to investigate how the partitioning of strain accommodation between these mechanisms may be expected to depend on experimental variables such as the normal stress, the particle size distribution, the layer thickness, the surface roughness of the sliding blocks, and even the sliding velocity.

Consider first the conditions under which a bridge will fail by frictional slip between its constituent particles. It

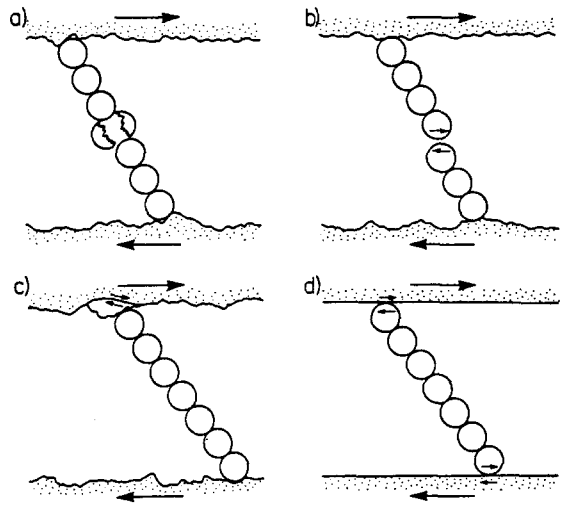

Fig. 20. Four failure modes of a grain bridge: (a) tensile failure of a particle under compressive loading; (b) slip between particles within a bridge; (c) failure of the sliding block surface which spalls new particles into the gouge layer; and (d) slip between a particle and the surface of the sliding block.

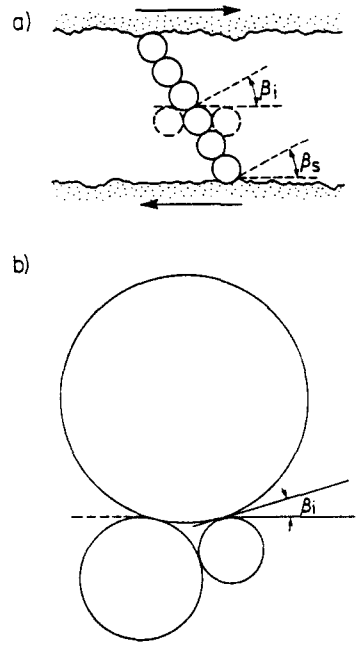

Fig. 21. (a) Simple two-dimensional grain bridge of identical particles showing the surface roughness angle β_s and the internal roughness angle β_i. (b) Nearest-neighbor geometry for a discrete, binary, fractal gouge (at any scale). Because nearest neighbors are different sizes at all scales, the internal roughness β_i for the fractal gouge is smaller than β_i for the gouge of identical particles in (a).

has long been recognized in soil mechanics that the apparent coefficient of friction, μ_{obs}, which is defined by the ratio of the applied shear to the normal stresses, is larger than the actual coefficient of friction between the particles. This increase in apparent friction is due to the misalignment between the interparticle slip planes and the macroscopic plane of shear displacement (Rowe 1962, Horne 1965). This misalignment also produces the shear dilatancy observed at low values of the normal stress. Scott (1963, pp. 293–304) derived a relationship for the apparent coefficient of friction for a hexagonal close-packed (hcp) array of equal spheres:

$$\mu_{obs} \equiv \frac{\sigma_s}{\sigma_n} = \frac{\sqrt{3} + 4\sqrt{2}\,\mu}{2(\sqrt{6} - \mu)}. \tag{8}$$

For example, if $\mu = 0.55$, then $\mu_{obs} = 1.27$ which is comparable to the peak stress ratio required to initiate sliding in a close packed sand at low σ_n where grain crushing is rare (Feda 1982).

For the purposes of the present discussion, consider the simple two-dimensional bridge of equal-sized particles in Fig. 21(a). Denote the angle between the macroscopic shear plane and the interparticle slip plane as β. By resolving the applied stress onto the slip plane, it may be shown that

$$\mu_{obs} = \frac{\mu + \tan\beta}{1 - \mu\tan\beta}. \tag{9}$$

Because β decreases once slip begins, the criterion for the failure of a bridge by frictional slip is

$$\frac{\sigma_s}{\sigma_n} \geq \frac{\mu + \tan\beta}{1 - \mu\tan\beta}. \tag{10}$$

The question of whether a bridge will fail by crushing a particle or by slip depends on the strength of the particles and the angle β. Particle strength and β both depend on the particle size distribution and the packing geometry.

Surface roughness may also be characterized by an average misalignment angle (which we denote β_s) between particles and surface asperities as illustrated in Fig. 21(a). It is determined by the relative scales of roughness and particle size. By analogy, the angle between particles within the gouge will be called the 'internal roughness' and denoted β_i. Equations (9) and (10) apply to both the surface roughness β_s as well as the internal roughness β_i. The question of whether a particular grain bridge fails by internal or surface slip depends upon the relative sizes of β_s and β_i.

For the smooth surfaces, the surface asperities are much smaller than the particles and β_s is close to zero. In this case equation (9) gives $\mu_{obs} \approx \mu$. Following a small initial adjustment of the particles, most bridges fail by slip at the gouge–rock interface. This may explain why the observed coefficient of friction is lower for the smooth surfaces than for any of the rough surface samples which must slip at a larger value of β_i. Slip at the interface for smooth surfaces may also explain why μ_{obs} is relatively independent of the particle distribution, and why the transient parameters do not significantly evolve with displacement. The dominance of slip over fracture also explains why smooth surfaces show more velocity weakening throughout the experiment than rough surfaces.

For the rough surfaces, β_s is comparable to or larger than β_i so slip may occur anywhere within the bridge. The angle β_i depends on the particle size distribution. Maximum β_i corresponds to an array in which all particles are the same size. For a two-dimensional array of close-packed identical cylinders, $\beta_i = 30°$; for a three-

dimensional hcp array, $\beta_i = 19.6°$ (Scott 1963, p. 298). We propose that minimum β_i corresponds to a fractal distribution with dimension 2.58. As discussed by Sammis *et al.* (1987), such a distribution minimizes the number of nearest neighbors, which are the same size *at all scales*. By so doing, it also minimizes the depth of the valleys in which the particles rest (and hence also minimizes β_i *at all scales*). We emphasize the requirement that β_i be minimized at all scales since it might seem intuitive that any infilling of the gaps between large particles with smaller particles might produce a smoother surface. This is not correct, the roughness depends on the *relative* sizes of all the particles which slide past each other. Figure 21(b) shows the nearest neighbor geometry (at any scale) for a discrete, fractal two-dimensional array of cylinders for which the diameter in successive size classes differs by a factor of 2. The fractal dimension is 1.58. Note that each particle rests in a valley between particles of the next two smaller classes. For this case, $\beta_i = 16°$. The angle for the equivalent three-dimensional fractal array of dimension 2.58 will be smaller still. Hence, as any initial particle distribution evolves toward a fractal one, it is expected that an increasing proportion of the bridges will fail by slip rather than fracture. This trend is enhanced by the decreased fracture probability in a fractal array associated with the decrease of nearest neighbors the same size at any scale.

The transition from velocity strengthening to velocity weakening observed in the rough surface experiments may reflect this evolution from a system which is dominated by fracture to one which is dominated by slip. Even after a fractal distribution is established and deformation is dominated by slip, the internal roughness β_i is still larger than $\beta_s = 0$ for the smooth surface. Hence μ_{obs} is always larger for rough surfaces than for smooth surfaces. The observation that a and b are also larger for the rough surfaces suggests that these transient parameters might be related to β, possibly through dilatational work.

A grain bridge fails when its weakest link fails. This weak link can be a particle which fails by fracture or a particularly low value of the internal angle β_i between two particles which slip. Obviously, the longer a grain bridge, the higher the probability of finding a weak link within it. Since a 1 mm layer of gouge has shorter bridges than a 3 mm layer, this may explain why the R1-series has a higher coefficient of friction that the R3-series as shown in Fig. 11. It is also interesting that the tendency for μ to decrease as the upper fractal limit increases in Fig. 11 reverses when the largest particle size is about $\frac{1}{3}$ of the layer thickness. This may also be a result of a statistical paucity of weakest links. Finally, note that for 1 mm thick layers, μ decreases again when the largest particle is about equal to the layer thickness. In this case bridges may not form.

The optical observation that more comminution has occurred in layers with rough surfaces than in those bounded by smooth surfaces supports this model (see Fig. 9). The transition from fracture-dominated deformation to slip-dominated deformation occurs at small displacements in the case of smooth surfaces. For the rough surfaces, this transition occurs throughout the experiment as evidenced by the continual evolution of the friction parameters with displacement.

DISCUSSION

The experimental program described above was designed to answer two questions: (1) how does the particle size distribution in a gouge evolve with increasing shear displacement? and (2) what is the frictional constitutive behavior of a fractal gouge with dimension 2.6, and how does it depend on the upper fractal limit? This second question was motivated by the observation that a natural fault gouge has a fractal geometry with $D = 2.6$.

The answer to the first question was simple and direct. As anticipated, a layer of gouge with an initially uniform particle distribution was observed to evolve into a fractal distribution having $D = 2.6$. Distributions which began with this fractal distribution maintained it. The answer to the second question was not so obvious. The most profound differences in frictional behavior were observed between rough and smooth sliding surfaces. This was true for the coefficient itself as well as its transient parameters. We conclude that these differences arise because shear strain in the gouge localizes at the interface with the smooth surfaces, but for the rough surfaces strain remains distributed across the layer. Observations which suggest localized sliding at the smooth surfaces include the constancy of the coefficient of friction and its transient parameters throughout an experimental run and their lack of dependence on the particle size distribution. We suggest that following the initial compaction (about 2 mm of displacement), relatively few additional grains are fractured. The large magnitude of the velocity weakening observed in this case is assumed to be a consequence of the dominance of slip over fracture.

The observation that the coefficient of friction depends on the thickness of the gouge layer argues against localization of the strain for the case of rough sliding surfaces. Support for this conclusion comes from the absence of evidence of localization in thin sections. The rough surfaces are not significantly smoothed at the end of the runs, and we find no evidence for the filling of rough surfaces by fine particles observed by Logan *et al.* (1979) for a calcite gouge between sandstone blocks. Such filling may require a more ductile gouge like calcite.

For the rough surfaces, the frictional behavior evolves from velocity strengthening to mild velocity weakening with increasing displacement. We propose that this behavior is a direct consequence of the evolution of the particle distribution toward a fractal arrangement which minimizes the number of same-size nearest neighbors at all scales. This geometry minimizes the probability that grains will fracture since each is cushioned by smaller particles. It also maximizes the probability of slip be-

tween particles by minimizing the depth of 'valleys' between adjacent particles at all scales. The evolution toward a fractal geometry thus produces a corresponding evolution from fracture toward slip which, in turn, produces the observed evolution from velocity strengthening toward velocity weakening.

It is important to recognize that, even though we prepare a gouge which has the same particle distribution as a fractal gouge, it does not have the proper spatial arrangement at the beginning of a run. Shear strain is still required to eliminate same-size nearest neighbors which result from the random initial packing. Our data suggest that less displacement is required to establish the spatial geometry if we begin with the appropriate fractal grain size distribution.

The formulation of a detailed micromechanical model for the frictional behavior of a layer of particulate material is beyond the scope of this paper. However, there is evidence that such a model should be based on 'grain bridges' which span the layer and carry the applied load. Such structures are commonly described in the soil mechanics literature. The continual formation and failure of bridges offers an explanation of how large displacements can be accommodated in the rough samples when no coherent slip planes are observed in thin section. The existence of such structures was previously postulated by Sammis *et al.* (1987) to explain how a self-similar gouge is established and maintained.

The strongest evidence for the existence of grain bridges in this data set is the observation of a larger coefficient of friction for thinner layers, and an increase in μ when the particle size is about one-third of the layer thickness. These observations, which are not adequately explained by continuum theory, are an expected consequence of a bridge model. If μ is determined by the strength of the bridges, and if bridges fail at their weakest element, then short bridges composed of a small number of potential failure elements are expected to be statistically stronger than long bridges.

The most surprising observation was that the transient parameters a and b are approximately three times as large for rough surfaces as for smooth. For smooth surfaces where slip dominates on the horizontal interface, these parameters are probably related to the velocity-induced changes in the fracture strength and lifetime of the adhesions described by classical friction theory. For rough surfaces, even when a fractal geometry is established and slip dominates, there is still a small misalignment angle between the interparticle slip planes and the sliding direction. There is experimental evidence that this misalignment may produce a velocity dependent dilatation (Morrow & Byerlee 1986). Large a and b values observed for rough surfaces may be associated with the stress required to produce such volume changes. A more quantitative discussion of these possibilities requires the formulation of a micromechanical model for the formation and failure of the grain bridges.

A central question in using laboratory friction parameters to describe natural faults is the uncertainty in scaling. For example, does the characteristic displacement of 10–50 μm observed in these experiments also apply to a natural fault, or is it a function of the laboratory particle size or surface roughness which should be scaled up to some relevant particle size or surface roughness in the natural fault? Sammis & Biegel (1989) proposed the upper fractal limit of the gouge particles as such a scaling parameter. The experiments reported here suggest that D_c is not very sensitive to the upper fractal limit. The strong dependence of D_c on normal stress suggests that it is probably related to the size of adhesions, and thus only indirectly related to the particle geometry, possibly through the number and geometry of stress-paths or grain bridges in the granular gouge.

Acknowledgements—This work was supported by National Science Foundation grant EAR-8608246.

REFERENCES

Allersma, H. G. 1982. Photo-elastic stress analysis and strains in simple shear. In: *Deformation and Failure of Granular Materials* (edited by Vermeer, P. A. & Luger, H. J.). A. A. Balkema, Rotterdam, 345–354.

Anderson, J. L., Osborne, R. H. & Palmer, D. F. 1982. Petrogenesis of cataclastic rock within the San Andreas fault zone of Southern California. *Tectonophysics*, **67**, 221–249.

Dieterich, J. H. 1978. Time-dependent friction and the mechanics of stick–slip. *Pure & Appl. Geophys.* **116**, 790–806.

Dieterich, J. H. 1979a. Modeling of rock friction: 1. Experimental results and constitutive equations. *J. geophys. Res.* **84**, 2161–2168.

Dieterich, J. H. 1979b. Modeling of rock friction: 2. Simulation of preseismic slip. *J. geophys. Res.* **84**, 2169–2175.

Dieterich, J. H. 1981. Constitutive properties of faults with simulated gouge. In: *Mechanical Behavior of Crustal Rocks. Geophys. Monogr. Am. Geophys. Un.* **24**, 108–120.

Feda, J. 1982. *Mechanics of Particulate Materials: The Principles.* Elsevier, New York.

Gallagher, J. J., Jr., Friedman, M., Handin, J. & Sowers, G. M. 1974. Experimental studies relating to microfracture in sandstone. *Tectonophysics* **21**, 203–247.

Horne, M. R. 1965. The behavior of an assembly of rotund, rigid, cohesionless particles. *Proc. R. Soc. Lond.* **A286**, 62–79.

Logan, J. M., Friedman, M., Higgs, N. G., Dengo, C. & Shimamoto, T. 1979. Experimental studies of simulated gouge and their application to studies of natural fault zones. *Proc. Conf. VIII, Analysis of Actual Fault Zones in Bedrock, U.S. geol. Surv., Open-File Rep.* **79–1239**, 305–343.

Mandl, G., de Jong, L. N. J. & Maltha, A. 1977. Shear zones in granular material: an experimental study of their structure and mechanical genesis. *Rock Mech.* **9**, 95–144.

Morgenstern, N. R. & Tchalenko, J. S. 1967. Microscopic structures in kaolin subjected to direct shear. *Géotechnique* **17**, 309–328.

Morrow, C. A. & Byerlee, J. D. 1986. The effect of velocity-dependent consolidation on the frictional strength of fault gouge. *Trans. Am. Geophys. Un.* **67**, 1187.

Oda, M. & Konishi, J. 1974. Microscopic deformation mechanisms of granular material in simple shear. *Soils and Foundations* **14**, 25–38.

Oda, M., Konishi, J. & Nemat-Nasser, S. 1982. Experimental micromechanical evaluation of strength of granular materials: effects of particle rolling. *Mechanics of Materials* **1**, 269–283.

Okubo, P. G. & Dieterich, J. H. 1986. State variable fault constitutive relations for dynamic slip. In: *Earthquake Source Mechanics* (edited by Das, S., Boatwright, J. & Scholz, C. H.). *Am. Geophys. Un. Geophys. Monogr.* **37**, 25–35.

Rice, J. R. & Gu, J. C. 1983. Earthquake after effects and triggered seismic phenomena. *Pure & Appl. Geophys.* **121**, 443–475.

Rowe, P. W. 1962. The stress–dilatancy relation for static equilibrium of an assembly of particles in contact. *Proc. R. Soc. Lond.* **A269**, 500.

Ruina, A. 1983. Slip instability and state variable friction laws. *J. geophys. Res.* **88**, 10,359–10,370.

Sammis, C., King, G. & Biegel, R. 1987. The kinematics of gouge deformation. *Pure & Appl. Geophys.* **125**, 777–812.

Sammis, C. & Biegel, R. In press. Fractals, fault gouge and friction. *Pure & Appl. Geophys.*

Scott, R. F. 1963. *Principles of Soil Mechanics*, Addison-Wesley, Reading, Massachusetts.

Tchalenko, J. S. 1968. The evolution of kink-bands and the development of compression textures in sheared clays. *Tectonophysics* **6**, 159–174.

Tchalenko, J. S. 1970. Similarities between shear zones of different magnitudes. *Bull. geol. Soc. Am.* **81**, 1625–1640.

Timoshenko, S. & Goodier, J. N. 1951. *Theory of Elasticity*. McGraw-Hill, New York.

Tullis, T. E. & Weeks, J. D. 1986. Constitutive behavior and stability of frictional sliding of granite. *Pure & Appl. Geophys.* **124**, 383–414.

Turcotte, D. L. 1986. Fractals and fragmentation. *J. geophys. Res.* **91**, 1921–1926.

Wu, F., Blatter, L. & Robertson, H. 1975. Clay gouges in the San Andreas fault system and their possible implications. *Pure & Appl. Geophys.* **113**, 87–96.